Energy gap of Kronig-Penney-type hydrogenated graphene superlattices

Joo-Hyoung Lee and Jeffrey C. Grossman
Department of Materials Science and Engineering, Massachusetts Institute of Technology, 77 Massachusetts Avenue, Cambridge, Massachusetts 02139
(Received 3 August 2011; published 27 September 2011)

The electronic structure of graphene-graphane superlattices with armchair interfaces is investigated with first-principles density-functional theory. By separately varying the widths, we find that the energy gap E_g is inversely proportional to the width of the graphene strip and that the gap increases as the hydrogenated strip becomes wider due to the enhanced confinement effect. It is further demonstrated that, unlike other graphene nanostructures, the superlattices exhibit both direct and indirect band gaps without external perturbations. This peculiarity in the nature of E_g originates from the different connection structures of the symmetrized wave function at the boundary between adjacent unit cells due to the reflection symmetry of the superlattices. These findings suggest that the optical as well as electronic properties of graphene superlattices can be controlled through selective chemical functionalization.

DOI: 10.1103/PhysRevB.84.113413 PACS number(s): 73.22.Pr

Carbon-based systems exhibit a rich variety of structures with equally intriguing physical properties in different dimensionality, which arises largely from the remarkable bonding flexibility of carbon atoms. Zero-dimensional fullerenes, one-dimensional (1-D) nanotubes, two-dimensional (2-D) graphene, and three-dimensional graphite are archetypical examples to name a few. Among these, graphene plays a special role because it serves as "the basis for understanding electronic properties in other allotropes"[1,2] and shows fascinating physical properties such as chiral integer Hall effect,[3,4] Klein tunneling,[5] and the absence of weak localization.[6] The origin of these exotic behaviors in graphene lies in the fact that the low-lying excitations around the Fermi point are described by massless, chiral Dirac fermions with a linear dispersion at the Fermi velocity v_F instead of the speed of light.[2]

Apart from its interesting fundamental physics, graphene has also been considered as a promising candidate for future electronics applications due to its high Fermi velocity, and numerous attempts have been made to control graphene's chemical and electrical properties.[7–12] Along this direction, there has been an increasing interest in graphene superlattices (GSLs) because their electronic structure can be modified geometrically,[13,14] as in graphene nanoribbons.[15–20] In particular, Kronig-Penney-like (KP) GSLs have brought about much excitement due to exotic transport properties. Park *et al.* demonstrated that the group velocity of the massless Dirac fermions is strongly renormalized in a highly anisotropic way because of the chiral nature of the electronic states.[21] Moreover, the chirality together with the quasi-1-D energy dispersion was predicted to make the electron wave packet propagate without spatial spreading, supercollimation, under a KP potential.[22] It was also found that the spin polarization of the tunneling conductance and magnetoresistance show an oscillatory behavior with the gate voltage.[23] While these works have revealed intriguing physics and a potential for graphene-based applications, a detailed study regarding the geometric effect of KP GSLs on the electronic structure is rare.

Recently, first-principles calculations demonstrated that the electronic structure of a narrow graphene strip carved out of the graphane matrix shows a very similar dependence on the interface type, as in graphene nanoribbons.[24] This indicates that the interfacial geometry between the potential barrier and graphene strip may also have a significant impact on the electronic properties in the case of KP GSLs. Furthermore, since it is now experimentally realizable to form patterned hydrogenation on graphene,[25] which would be readily extended to the synthesis of the KP GSLs, it is of interest to achieve an improved understanding of the geometric effect on the electronic structure of the GSLs both from a fundamental physics standpoint and for future graphene-based applications.

In the present work, we have performed first-principles studies on the electronic structure of KP GSLs with armchair-type interfaces (AGSLs) based on density-functional theory (DFT). AGSLs are modeled with a repeated structure of pure and hydrogenated graphene (i.e., graphane) strips, and calculations are carried out by varying the widths of the pure and hydrogenated parts separately. Our results demonstrate that AGSLs possess finite energy gaps that increase as the graphane region becomes wider due to the enhanced confinement effect. Surprisingly, the band gaps exhibit both direct and indirect character depending on the width of the graphane strip, and we show that the origin of this peculiarity in the band gap lies in the symmetry of AGSLs, which governs the connection structure of the wave functions at the boundary between neighboring unit cells.

All first-principles calculations are performed within DFT as implemented in the Vienna Ab Initio Simulation Package,[26] employing 450-eV plane-wave cutoff, Vanderbilt-type ultrasoft pseudopotentials,[27] and the exchange-correlation energy is treated within the generalized gradient approximation (GGA) of Perdew and Wang.[28] The interlayer separation is kept at 18 Å to avoid spurious interactions between the superlattice layers, and the Brillouin-zone (BZ) integration is carried out by employing the Gaussian smearing approach with a smearing parameter of 0.05 eV. Due to the variation in the cell size, different numbers of irreducible $\mathbf{k}$ points ($N_{\mathbf{k}}$) are considered: for the smallest cell, $N_{\mathbf{k}} = 256$ is used, whereas it gradually decreases to 96 as the cell becomes larger.

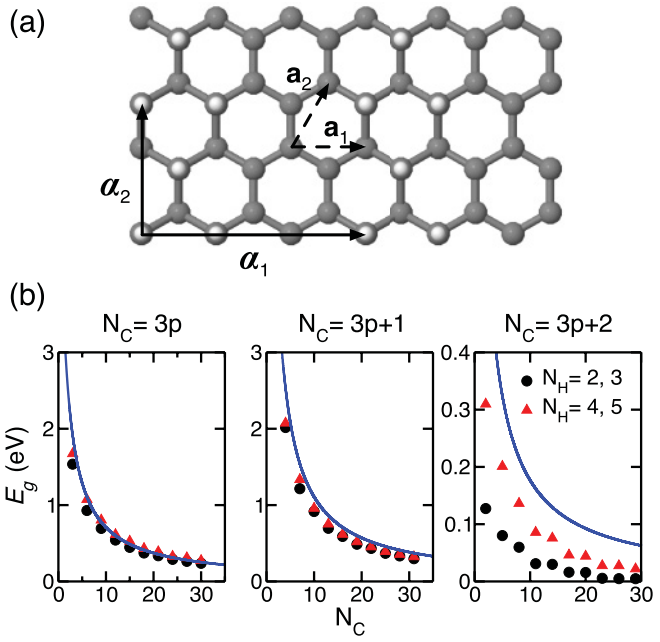

FIG. 1. (Color online) (a) Structure of armchair GSLs (AGSLs) for $(N_H, N_C) = (3,3)$. $\boldsymbol{\alpha}_1$ and $\boldsymbol{\alpha}_2$ are lattice vectors of AGSLs, and those of pure graphene are shown as $\mathbf{a}_1$ and $\mathbf{a}_2$, respectively, for comparison. C and H atoms are represented in gray and white spheres, respectively. (b) E_g (in eV) of AGSLs as a function of N_C for different N_H values: $N_C = 3p$ (left), $N_C = 3p+1$ (middle), and (c) $N_C = 3p+2$ (right). Solid curves are the energy gaps of armchair graphene nanoribbons (AGNRs).[16]

Figure 1(a) shows the geometry of AGSLs employed in the present work, which are composed of alternating arrangements of graphene and graphane strips. Lattice vectors of AGSLs ($\boldsymbol{\alpha}_1$ and $\boldsymbol{\alpha}_2$) and pure graphene ($\mathbf{a}_1$ and $\mathbf{a}_2$) are also shown in Fig. 1. Here, the "chairlike" dual hydrogenation is considered because this structure is shown to have a higher binding energy than other hydrogenated graphene structures.[29] As in graphene nanoribbons (GNRs), the system size of AGSLs is represented by the numbers of pure (N_C) and hydrogenated (N_H) carbon dimers along $\boldsymbol{\alpha}_2$ in the unit cell. For instance, the AGSL in Fig. 1 has $(N_H, N_C) = (3,3)$.

We first compute the energy gaps (E_g) of AGSLs as a function of N_C for different values of N_H, shown in Fig. 1(b). Because of the rectangular unit cell of AGSLs, the Dirac point of pure graphene is mapped onto either the Γ point or two-thirds along the $\Gamma \rightarrow$ X direction (referred to as $2/3\,\overrightarrow{\Gamma X}$), depending on the magnitude of $\boldsymbol{\alpha}_1$. One might thus expect that the conduction and valence band (VB) would meet at these points. As can be seen, however, E_g always remains nonzero regardless of the N_H and N_C values, which is in contrast with recent effective Hamiltonian studies in which a KP potential preserves the semimetallic nature of the graphene and introduces extra Dirac points in the Brillouin zone.[21,30]

We also find a similar variation in the C-C dimer length, d_C, along $\boldsymbol{\alpha}_2$ within the graphene strip: d_C is found to decrease by $2.1 - 2.8\%$ at the interface and quickly restores the C-C bond length in graphene strips. This situation is very similar to AGNRs, in which the C-C dimer length at the edge decreases by 3.5% compared with that at the ribbon center. This reduction leads to a 12% increase in the hopping parameter, which was shown to play a critical role in opening the gap.[16] These observations indicate that the gap in AGSLs is the result of the confinement effect due to the potential barrier from the hydrogenated strips and structural relaxation at the interface as well.

We note that the gap is categorized into three different families, as in the case of AGNRs,[15,16] as is clearly seen from Fig. 1(b). For a fixed N_H, the magnitude of E_g is well ordered depending on the values of N_C: $E_g(N_C = 3p+1) > E_g(N_C = 3p) > E_g(N_C = 3p+2)$, where p are integers. Furthermore, E_g is well fitted with $N_C^{-\beta}$, where $0.74 < \beta < 0.90$ depending on N_H values. From Fig. 1(b), it is found that E_g increases with N_H for a given N_C, due to wider potential barriers provided by the graphane strip with larger N_H values. By computing $\Delta E_g = E_g(N_H = 4,5) - E_g(N_H = 2,3)$, it is found that, although there exist three different families in E_g, ΔE_g remain close to each other among them, implying that the confinement effect is very similar. This similarity in ΔE_g results in the relative increase in the gap of 14 and 6% on average for $N_C = 3p$ and $3p+1$, respectively, whereas the small gap makes $E_g(N_C = 3p+2)$ for $N_H = 4,5$ more than doubled from those with $N_H = 2,3$.

The variation in E_g with respect to N_C can also be compared with that of AGNRs. As is seen from Fig. 1(b), E_g of AGSLs is close to the energy gap in AGNRs. For instance, E_g with $N_C = 3p$ and $3p+1$ for $N_H = 2$ and 3 is reduced from that of AGNRs by 10 and 19% on average, respectively, whereas the reduction is as large as 83% when $N_C = 3p+2$. However, the difference is reduced by as low as 4, 14, and 50% for $N_C = 3p$, $3p+1$, and $3p+2$, respectively, in the case of $N_H = 4$ and 5, due to the wider potential barrier. The similarity in E_g partly implies that the hydrogenated strips isolate the graphene regions so that the electronic structure of the latter resembles that of AGNRs. It should be noted, however, that the periodic nature of the potential barrier significantly differentiates AGSLs from AGNRs, as is discussed below.

In order to better understand the nature of these energy gaps, we plot the band structures of the AGSLs in Fig. 2 for selected (N_H, N_C) values. It is clear from Fig. 2 that the bands in the $\Gamma \rightarrow$ Y direction are highly dispersive, whereas they are quite flat along $\Gamma \rightarrow$ X. This implies a higher electrical conductivity along than across the potential barrier, leading to an anisotropic behavior in the transport properties.

Surprisingly, unlike AGNRs, in which both the conduction-band minimum (CBM) and valence-band maximum (VBM) occur at the Γ point in the Brillouin zone (BZ),[16] the CBM and VBM of AGSLs are located at either the Γ or X point in the BZ, depending on the detailed superlattice geometry. As previously mentioned, since the Dirac point of graphene is mapped onto either Γ or $2/3\,\overrightarrow{\Gamma X}$ in AGSLs, the *direct* band gap is expected around these points due to the confining potential. This is exactly the case for even N_H values, in which both the VBM and CBM are at the same $\mathbf{k}$ point, as shown in Fig 2(a). When N_H assumes odd values, however, indirect as well as direct band gaps are obtained, as presented in Fig. 2(b). With $N_H = 3$, for instance, the VBM (CBM) occurs at the X (Γ), X (Γ), and Γ (X) points when $N_C = 3p$, $3p+1$, and $3p+2$, respectively, which is the same for $N_H = 7$, whereas

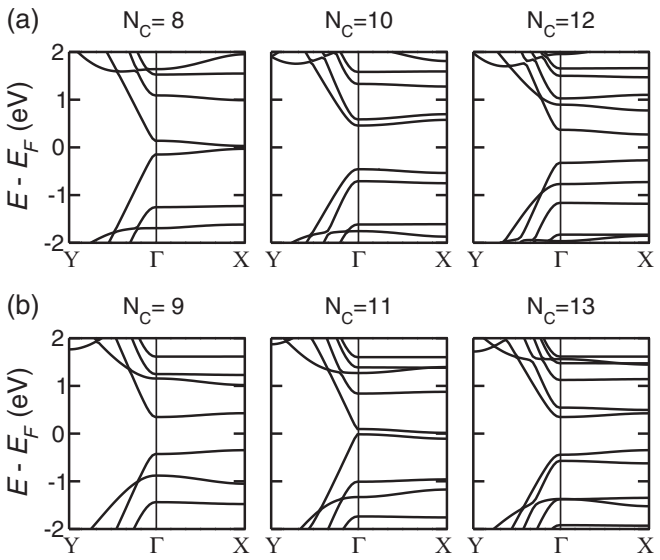

FIG. 2. Band structures of AGSLs for selected N_C values with (a) $N_H = 2$ and (b) $N_H = 3$. X $= (\pi/|\boldsymbol{\alpha}_1|,0)$ and Y $= (0,\pi/|\boldsymbol{\alpha}_2|)$.

direct gaps occur when $N_H = 5$. We note that the difference in the energy eigenvalues at the Γ and X points for $N_H = 9$ becomes less than 1 meV due to the wide potential barrier, making the dispersion along Γ → X flat, essentially resulting in a set of AGNRs. It should be stressed that, while indirect band gaps can be induced in AGNRs by applying an external bias[31] and in bilayer graphene through strain,[32] the indirect band gap in AGSLs is an intrinsic effect in the sense that no external perturbation is required.

To understand the origin of the indirect gap in AGSLs for odd N_H values, we plot the real part of the wave function ψ at the Γ (ψ_Γ) and X point (ψ_X) for $(N_H,N_C) = (3,5)$ and $(5,5)$ in Figs. 3 and 4, respectively. In Figs. 3 and 4, the wave functions for both the top of the valence band ($\psi^{VB}_{\Gamma,X}$) and bottom of the conduction band ($\psi^{CB}_{\Gamma,X}$) are presented. As is seen from both figures, $\psi_{\Gamma,X}$ is antisymmetric with respect to the reflection plane P_ρ, which is represented with the dotted line in the figures. In fact, $\psi_{\Gamma,X}$ becomes symmetric and antisymmetric when $N_C = 4p - 1$ and $4p + 1$, respectively. This symmetry property of $\psi_{\Gamma,X}$ is the result of the reflection symmetry of AGSLs for odd N_H values.

We first note that the reflection σ with respect to P_ρ is a covering operation of the 2-D Hamiltonian of the AGSLs ($\mathscr{H}_{AGSL}$) when $N_H = 2p + 1$: $\sigma\mathscr{H}_{AGSL} = \mathscr{H}_{AGSL}\sigma$. Thus, if $\psi_{\Gamma,X}$ is a nondegenerate eigenfunction of $\mathscr{H}_{AGSL}$, which is indeed the case, it is easy to see that $\sigma\psi_\Gamma = \pm\psi_\Gamma$. To show the nondegeneracy of ψ_Γ, let us consider the space group $\mathscr{G}$ of AGSLs, which is the same as the group of a $\mathbf{k}$ vector at the Γ and X points. We find that $\mathscr{G}$ of the fully relaxed superlattices consists of four elements: E (identity), σ, i (inversion), and C_2 (π rotation about the x axis). Since each of these elements forms its own class, there are four 1-D irreducible representations of $\mathscr{G}$, which only allows nondegenerate eigenfunctions of $\mathscr{H}_{AGSL}$.

The symmetrized wave functions form different node structures at the connection regions (the solid rectangles in Figs. 3 and 4) between adjacent unit cells, depending on N_H

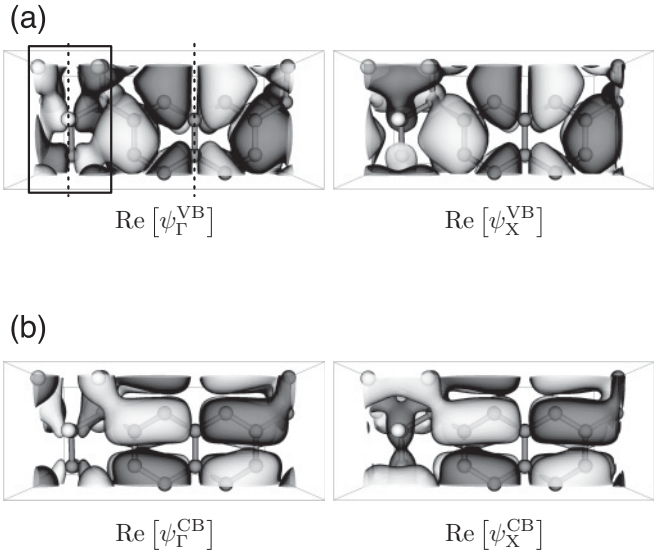

FIG. 3. Isosurfaces of the real part of the wave function at the Γ and X points with $(N_H,N_C) = (3,5)$ for the (a) top of the valence band (VB) and (b) bottom of the conduction band, respectively. Light and dark gray surfaces are generated at +10 and −10% of the maximum value, respectively. The dotted line and solid square represent the plane for the reflection symmetry and the graphane region, where wave functions from the adjacent cell are connected, respectively.

values. As is seen from Figs. 3(a) and 3(b), both ψ^{VB} and ψ^{CB} for $(N_H,N_C) = (3,5)$ have the same number of nodes N_n at the Γ point, whereas N_n is reduced at the X point, leading to a lowering of the kinetic energy. This change in N_n thus places the VBM and CBM at the Γ and X points, respectively. We also computed ψ for $(N_H,N_C) = (3,7)$ and found that N_n is increased at the X point, reversing the result with $(N_H,N_C) = (3,5)$: the VBM occurs at the X point, whereas the CBM is at the Γ point.

The situation for $N_H = 5$ is, however, in sharp contrast with the above case, as depicted in Fig. 4. From Fig. 4(a), it is seen that N_n is decreased going from the Γ to the X point in the VB, which makes the Γ point the VBM. In contrast, ψ^{CB}_Γ has

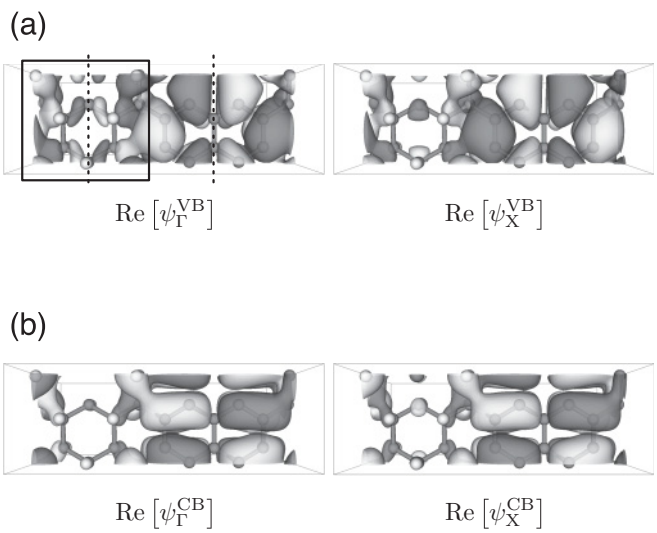

FIG. 4. Same as Fig. 3 with $(N_H,N_C) = (5,5)$.

a fewer number of nodes than ψ_X^{CB}, implying that the energy eigenvalue at the Γ point is smaller than that of the X point in the CB and thus forming a direct band gap at the Γ point for $(N_H, N_C) = (5,5)$. The wave function with $N_C = 7$ is also examined, and it is found that N_n is larger (smaller) at the X point in the VB (CB), resulting in the direct gap at the X point.

In this work, we have performed first-principles studies on the electronic structure of graphene/graphane superlattices with armchair-type interfaces. Through separately varying the widths of graphene and graphane strips, it was demonstrated that the superlattices exhibit nonzero band gaps, which are categorized into three different families depending on the strip widths. We further showed that the gap of AGSLs becomes indirect due to the reflection symmetry of the superlattice for a particular set of graphane widths, which would lead to novel optical properties. The appearance of the indirect gap is not limited to armchair interfaces, and other KP-type superlattices will also develop indirect gaps as long as the structure contains a reflection symmetry.

While the gap in AGSLs arises from a combined effect of quantum confinement and structural relaxation, the model Hamiltonian in Ref. 16 is not directly applicable to AGSLs to describe quantitative behavior of the gap in AGSLs. This is because the Hamiltonian was developed for a system with a gap only at the Γ point, whereas the VBM and CBM occur both at the Γ and X points in AGSLs. However, when the graphane strips become wider (for instance, $N_H \geqslant 9$), the difference in the energy eigenvalues at the Γ and X points becomes small ($\leqslant 1$ meV), making the energy dispersion flat along $\Gamma \rightarrow$ X. Under this circumstance, the graphene strips are isolated and effectively the same as nanoribbons, as is manifested in Fig. 1(b), where the gap of AGSLs approaches that of AGNRs. In this case, the model Hamiltonian in Ref. 16 can be invoked to explain the behavior of the gap as a function of the graphene width.

Recently, superlattice structures with broken inversion symmetry were proposed to induce a finite gap at the Dirac point in graphene.[13] Our results, however, demonstrate that graphene superlattices can have nonzero band gaps even with the inversion symmetry if a sufficient confining potential is present. We note that, since the energy gaps in the present work were computed within DFT-GGA, beyond-GGA approaches such as hybrid functionals or GW approximation will produce larger gaps. Despite this underestimation, however, the trend in E_g with N_C and N_H values will remain valid even within GGA, as demonstrated elsewhere.[33]

We are grateful for support from the Massachusetts Institute of Technology Energy Initiative seed grant program.

[1] A. K. Geim and K. S. Novoselov, Nat. Mater. **6**, 183 (2007).
[2] A. H. C. Neto, F. Guinea, N. M. R. Peres, K. S. Novoselov, and A. K. Geim, Rev. Mod. Phys. **81**, 109 (2009).
[3] K. S. Novoselov, A. K. Geim, S. V. Morozov, D. Jiang, M. I. Katnelson, I. V. Grigorieva, S. V. Dubonos, and A. A. Firsov, Nature (London) **438**, 197 (2005).
[4] Y. B. Zhang, Y. W. Tan, H. L. Stormer, and P. Kim, Nature (London) **438**, 201 (2005).
[5] M. I. Katnelson, K. S. Novoselov, and A. K. Geim, Nat. Phys. **2**, 620 (2006).
[6] S. V. Mozorov, K. S. Novoselov, M. I. Katsnelson, F. Schedin, L. A. Ponomarenko, D. Jiang, and A. K. Geim, Phys. Rev. Lett. **97**, 016801 (2006).
[7] M. Calandra and F. Mauri, Phys. Rev. B **76**, 161406(R) (2007).
[8] I. Calizo, W. Bao, F. Miao, C. N. Lau, and A. A. Balandin, Appl. Phys. Lett. **91**, 201904 (2007).
[9] H. Sevinçli, M. Topsakal, E. Durgun, and S. Ciraci, Phys. Rev. B **77**, 195434 (2008).
[10] M. T. Lusk and L. D. Carr, Phys. Rev. Lett. **100**, 175503 (2008).
[11] X. Dong *et al.*, Phys. Rev. Lett. **102**, 135501 (2009).
[12] J. Berashevich and T. Chakraborty, Phys. Rev. B **80**, 033404 (2009).
[13] R. P. Tiwari and D. Stroud, Phys. Rev. B **79**, 205435 (2009).
[14] W. Liu, Z. F. Wang, Q. W. Shi, J. Yang, and F. Liu, Phys. Rev. B **80**, 233405 (2009).
[15] V. Barone, O. Hod, and G. E. Scuseria, Nano Lett. **6**, 2748 (2006).
[16] Y.-W. Son, M. L. Cohen, and S. G. Louie, Phys. Rev. Lett. **97**, 216803 (2006).
[17] T. Wassmann, A. P. Seitsonen, A. M. Saitta, M. Lazzeri, and F. Mauri, Phys. Rev. Lett. **101**, 096402 (2008).
[18] L. Jiao, L. Zhang, X. Wang, G. Diankov, and H. Dai, Nature (London) **458**, 877 (2009).
[19] K. Suenaga and M. Koshino, Nature (London) **468**, 1088 (2010).
[20] Z. Hou, X. Wang, T. Ikeda, S.-F. Huang, K. Terakura, M. Boero, M. Oshima, M.-A. Kakimoto, and S. Miyata, J. Phys. Chem. C **115**, 5392 (2011).
[21] C.-H. Park, L. Yang, S.-W. Son, M. L. Cohen, and S. G. Louie, Nat. Phys. **4**, 213 (2008).
[22] C.-H. Park, S.-W. Son, L. Yang, M. L. Cohen, and S. G. Louie, Nano Lett. **8**, 2920 (2008).
[23] Z. P. Niu, F. X. Li, B. G. Wang, L. Sheng, and D. Y. Xing, Eur. Phys. J. B **66**, 245 (2008).
[24] A. K. Singh and B. I. Yakobson, Nano Lett. **9**, 1540 (2009).
[25] R. Balog, B. Jørgensen, L. Nilsson, M. Andersen, E. Rienks, M. Bianchi, M. Fanetti, E. Lægsgaard, A. Baraldi, S. Lizzit, Z. Sljivancanin, F. Besenbacher, B. Hammer, T. G. Pedersen, P. Hofmann, and L. Hornekær, Nat. Mater. **9**, 315 (2010).
[26] G. Kresse and J. Furthmuller, Phys. Rev. B **54**, 11169 (1996).
[27] D. Vanderbilt, Phys. Rev. B **41**, 7892 (1990).
[28] J. P. Perdew and Y. Wang, Phys. Rev. B **45**, 13244 (1992).
[29] J. O. Sofo, A. S. Chaudhari, and G. D. Barber, Phys. Rev. **75**, 153401 (2007).
[30] M. Barbier, P. Vasilopoulos, and F. M. Peeters, Phys. Rev. B **81**, 075438 (2010).
[31] K. Majumdar, K. V. R. M. Murali, N. Bhat, and Y.-M. Lin, Nano Lett. **10**, 2857 (2010).
[32] S.-M. Choi, S.-H. Jhi, and Y.-W. Son, Nano Lett. **10**, 3486 (2010).
[33] L. Pisani, J. A. Chan, B. Montanari, and N. M. Harrison, Phys. Rev. B **75**, 064418 (2007).